Organic Electronics 13 (2012) 399–408

Contents lists available at SciVerse ScienceDirect

Organic Electronics

journal homepage: www.elsevier.com/locate/orgel

Theoretical characterization of the TTF/Au (1 1 1) interface: STM imaging, band alignment and charging energy

J.I. Martínez [a,*], E. Abad [a], C. González [b], J. Ortega [a], F. Flores [a]

[a] Departmento de Física Teórica de la Materia Condensada, Universidad Autónoma de Madrid, ES-28049 Madrid, Spain
[b] Departamento de Superficies y Recubrimientos, Instituto de Ciencia de Materiales de Madrid (CSIC), ES-28049 Madrid, Spain

ARTICLE INFO

Article history:
Received 13 April 2011
Received in revised form 2 December 2011
Accepted 4 December 2011
Available online 15 December 2011

Keywords:
Density functional theory
Metal/organic interfaces
TTF
Theoretical STM
Charging energy

ABSTRACT

A detailed density functional study is performed to analyze the TTF/Au (1 1 1) interface, including the effect of the molecular charging energy on the transport gap. Theoretical STM calculations are carried out, and compared with recent STM experimental evidence, for a dilute TTF/Au (1 1 1) structure in order to validate the interface geometry used in our calculations. We show that the alignment between the metal and the organic levels is mainly controlled by the charge transfer between the two materials, as determined by the difference between the molecule Charge Neutrality Level (*CNL*), and the initial Fermi level. The calculated transport gap is 4.1 eV, and the *CNL* is found close to the LUMO level, located about 0.7 eV from vacuum.

1. Introduction

Understanding the interaction between organic molecules and metal surfaces is of paramount importance in diverse fields such as organic electronics, molecular electronics, catalysis, surface photochemistry. In particular, the growing field of organic electronics relies on the use of organic conjugated molecules as components of multilayer devices. The performance of these devices depends critically on the energy barriers that control the carrier transport between layers, energy barriers that are determined by the relative alignment of the molecular levels at metal–organic (MO) or organic–organic (OO) interfaces [1,2].

Molecular level alignment at organic junctions has been widely investigated in the last decade [3–5]. Since the Schottky–Mott limit (where use of the vacuum level alignment is made) was disproved [6,7], many different mechanisms have been proposed to explain the barrier formation at MO interfaces: chemical reactions and the formation of gap states in the organic gap [3,5,8,9]; orientation of molecular dipoles [10,11]; or compression of the metal electron tails at the MO interface due to the Pauli repulsion [9,12–14]. It has been suggested that the tendency of the Charge Neutrality Level (*CNL*) of the organic material to align with the interface Fermi level [15,16] plays also an important role; this mechanism is associated with the induced density of interface states (IDIS) in the organic gap and the charge transfer between the organic and the metal. More recently, this model has been extended to the Unified-IDIS model by inclusion of Pauli repulsion and intrinsic molecular dipoles [14,17,18]. We also mention the integer charge transfer (ICT) model, where polaronic states in the organic material are assumed to modify the charge transfer mechanism, creating spontaneous integer charge transfer at the interface [19]. For atomically "dirty" interfaces see reference [20].

Theoretical studies of MO interfaces are usually based on density functional theory calculations. It is well-known, however, that standard DFT methods present important practical problems for an accurate simulation of the organic-molecule/metal interaction. First, in these calculations the Kohn–Sham single-particle eigenvalues do not properly describe the electronic energy levels of the sys-

* Corresponding author.
E-mail addresses: joseignacio.martinez@uam.es (J.I. Martínez), enrique.abad@uam.es (E. Abad), cesar.gonzalez@icmm.csic.es (C. González), jose.ortega@uam.es (J. Ortega), fernando.flores@uam.es (F. Flores).

1566-1199/$ - see front matter © 2011 Elsevier B.V. All rights reserved.
doi:10.1016/j.orgel.2011.12.003

tem, and in particular yield a transport gap (or HOMO–LUMO gap) that is too small [21,18]. A second problem is the poor description of weak interactions (e.g. van der Waals forces) in these calculations, resulting in many cases in a non-reliable molecule/surface adsorption geometry. Finally, these molecule–metal systems are usually large, requiring the use of computationally efficient DFT techniques.

In this paper we consider the paradigmatic case of a TTF/Au (1 1 1) interface, and analyze its MO barrier height as well as its molecular adsorption geometry. Tetrathiofulvalene (TTF) is a prototypical electron donor organic molecule. Recent experiments show that TTF molecules on Au (1 1 1) form a superlattice of monomers spaced a distance ranging between several nanometers apart to closepack monolayered structures [22,23]. In this case the molecule/metal interaction is weak and we find that a reliable description of the TTF geometry at the interface cannot be accurately achieved using conventional DFT-calculations [22,24]. For this reason, we have analyzed the TTF geometry by comparing experimental STM-images [22] with a detailed calculation of the tunneling currents; in this approach we obtain the TTF geometry by fitting the theoretical calculations to the experimental image. Once we obtain the molecule adsorption geometry we analyze the molecule density of states (DOS), the charge transfer, the interface dipole and other properties related to the TTF/Au (1 1 1) interface, and discuss how the interface barrier evolves when going from the isolated molecule to the full monolayer case. In these calculations, we combine a local-orbital LDA–DFT with a calculation of the charging energy, U, of the molecule on the surface, to correct the LDA energy spectrum and obtain the appropriate transport energy gap.

2. TTF/Au interaction: DFT calculations and charging energy

2.1. Method of calculation

Fig. 1 shows the systems and geometries we are interested in: an isolated TTF-molecule deposited on 7 × 7-Au (1 1 1) cluster (Fig. 1A); and two different periodic TTF layers on a Au (1 1 1) surface. We have considered the 6 × 6 [4] (Fig. 1B) and the herringbone (HB) 6 × 3 geometries [5] (Fig. 1C); this approach will allow us to analyze how the interface properties depend on the layer coverage.

In our calculations, the case of a single TTF molecule on Au (1 1 1) was simulated by means of a cluster of 196 Au atoms, with four Au-layers and 49 atoms per layer, with a 7 × 7 arrangement and no periodicity (see Fig. 1A); it has been checked that this cluster size is enough to avoid border effects (as tested by calculating density of states – DOS – profiles projected on the molecular orbitals). The dilute 6 × 6 geometry (see Fig. 1B) represents a periodic layer with a distance between neighboring TTF molecules large enough to ensure that they do not interact with each other. The geometry used in our calculations for the herringbone monolayer case (see Fig. 1C) has been constructed based on a recent STM experiment by Yan and coworkers [23], and it has been modeled as a 6 × 3-periodicity lattice with two TTF molecules per unit cell. In all these cases, we assume that the TTF adsorption geometry corresponds to the one obtained through our STM analysis (see Section 3 and Figs. 1D, 2). All the calculations were performed for slabs of four and six Au-layers; in particular, we found that four Au-layers are enough to obtain converged results for the electronic structure. The Brillouin zones of both the 6 × 6 and 6 × 3 periodicities were sampled with 4 × 4 × 1 Monkhorst–Pack grids [25]. Since FIREBALL is a real-space technique there is no practical limitation on the value for the distance between slabs in the $\hat{\mathbf{z}}$ direction; in these calculations we have chosen a distance of 99 Å so different slabs cannot virtually see each other.

We analyze all these cases by means of a very efficient local-orbital DFT technique (FIREBALL) [26–28]. In these calculations we use the LDA exchange–correlation functional, and a basis set of optimized numerical atomic orbitals (NAOs) [29,30] is used to represent the valence electrons, whilst the core electrons are taken into account by means of norm-conserving scalar-relativistic pseudopotentials [31]. A basis set of sp^3d^5 NAOs for C, S and Au, and s for H, have been considered in the calculations, with the

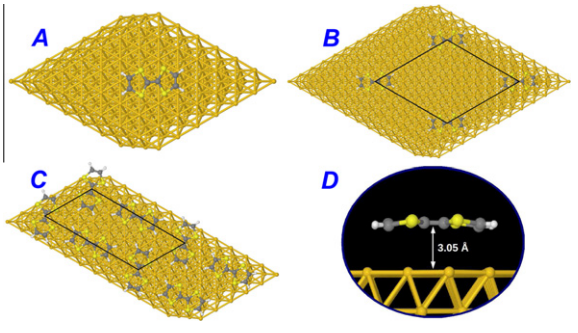

Fig. 1. TTF monolayers on the Au (1 1 1) surface: (A) cluster model; (B) dilute structure ($\mathbf{a} = \mathbf{b} = 17.56$ Å, $\widehat{\mathbf{ab}}=60^\circ$); (C) herringbone structure ($\mathbf{a} = 17.56$ Å and $\mathbf{b} = 8.78$ Å, $\widehat{\mathbf{ab}} = 60^\circ$); and (D) side view of a TTF molecule on the Au (1 1 1) surface, as obtained in our theoretical STM analysis, see Fig. 2. For (B and C), the solid lines denote the surface unit cells used in the calculations.

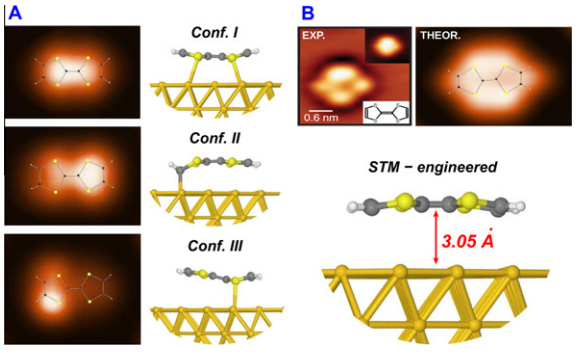

Fig. 2. (A) Theoretical STM images of TTF on Au (1 1 1) surface for three different configurations (explained in the text); a side view for each structure is also shown. (B) (upper panel) comparison between the experimental [22] and our optimized theoretical STM images (all of them for $V_s = -1V$); (lower panel) side view of the our STM-optimized TTF atomic structure on Au (1 1 1).

following cut-off radii (in a.u.): $s = 4.0$, $p = 4.5$, $d = 5.4$ (C), $s = 4.2$, $p = 4.7$, $d = 5.5$ (S), $s = 4.5$, $p = 4.9$, $d = 4.3$ (Au) and $s = 4.1$ (H). This basis set has been optimized to yield a good description of the electronic band structure as well as atomic structure for the Au bulk-phase, and has been widely tested and used in previous studies on the interaction of Au-tips with C_{60}, and TCNQ/Au and C_6H_6/Au interfaces [32–35]. For the TTF molecule this calculational approach yields C–C nearest-neighbor distances of 1.40 and 1.47 Å – to be compared with 1.39 and 1.44 Å obtained by a plane-wave DFT implementation [4], and experimental values of 1.40 and 1.45 Å [28] – (no available data for the C–H and S–C experimental bond-lengths), and a LDA-calculated HOMO/LUMO gap of 3.3 eV – to be compared with 2.6 eV for converged basis set LDA or GGA calculations [22].

The main inaccuracy of using a non-converged basis set of NAOs, once the basis has been optimized for each subsystem, appears in the relative misalignment found for the electronic levels of both materials (a misalignment that might also appear even for a converged basis set). Then, in order to have the Au and TTF levels correctly aligned initially at the experimental value, we shift by ε_0 the molecular levels of TTF, using the shift Hamiltonian $\mathbf{O}^{shift} = \sum \varepsilon_0 |\mu_i\rangle\langle\mu_i|(|\mu_i\rangle$ being the eigenstates of the isolated molecule), which can be thought of a pseudopotential. Its net effect is move rigidly the TTF spectra, allowing us to align it correctly with the gold band structure. In our calculations we have assumed that the TTF midgap is initially located 2.8 eV below the metal workfunction (5.3 eV). This value is obtained from accurate calculations for the HOMO/LUMO levels of the TTF molecule, as described in Section 2.2.

We also mention that our FIREBALL calculations use a self-consistent version [36] of the Harris–Foulkes [37,38] functional. In this approximation this potential is calculated by approximating in a self-consistent fashion the total charge by a superposition of spherical charges around each atom. This neglects off-diagonal contributions of the induced charge (dipolar contributions) whose effects, although not important for the self-consistent calculation itself, introduces non-negligible contributions to the induced Hartree potential. One of these effects is due to the induced "pillow" dipole (so-called Pauli effect) [39], which is created by the compression of the electron metal tails due to their overlap with the organic molecule wave-functions. The second effect we consider in this paper is associated with the charge induced on the metal surface and the accompanying induced "metal surface" dipole, that tends to shift that surface charge from practically the last metal layer to the image plane located outwards. More details about these effects are discussed in the Appendix.

2.2. Charging energy and energy gap

For a gas-phase molecule, an accurate calculation of its transport gap (or HOMO–LUMO gap) can be obtained as the difference between the electron affinity, $EA = -\varepsilon_{\mathrm{LUMO}} = E[N] - E[N+1]$, and ionization potential, $IP = -\varepsilon_{\mathrm{HOMO}} = E[N-1] - E[N]$, where $E[N_i]$ is the total energy for a neutral (N) or charged ($N \pm 1$) molecule with N_i electrons:

$$E^t(gas) = \varepsilon_{\mathrm{LUMO}} - \varepsilon_{\mathrm{HOMO}} = E[N+1] + E[N-1] - 2E[N] \quad (1)$$

In the case of the TTF molecule we have obtained $E^t(gas)$ using the real-space OCTOPUS code [40], the accurate hybrid GGA-PBE0 exchange–correlation functional [41] and Eq. (1); this yields $EA = -0.64$ eV, $IP = 5.67$ eV and $E^t(gas) = 6.3$ eV (TTF gas-phase). We also mention that using Eq. (1) together with LDA FIREBALL calculations with the basis set described in Section 2 yields an affinity/ionization gap of 8.19 eV for the TTF molecule.

As mentioned above, in standard DFT calculations the Kohn–Sham (KS) eigenvalues do not properly describe the electronic energy levels of the system, and transport gaps that are usually too small. For example, LDA or GGA calculations for TTF molecule yield a HOMO–LUMO KS gap of only 2.6 eV. Using Janak's theorem [42] and a kind of LSDA + U functional for the exact DFT energy, Sau et al. [43] have shown that the molecular HOMO and LUMO levels are given by:

$$\begin{aligned} E(\mathrm{LUMO}) &= E^{\mathrm{KS}}(\mathrm{LUMO}) + \frac{U_0^{\mathrm{LUMO}}}{2} \\ E(\mathrm{HOMO}) &= E^{\mathrm{KS}}(\mathrm{HOMO}) - \frac{U_0^{\mathrm{HOMO}}}{2}, \end{aligned} \quad (2)$$

where $E^{\mathrm{KS}}(\alpha)$ are the LDA KS levels and U_0^{α} the corresponding charging energies. Moreover, the following equations [43]:

$$\begin{aligned} U_0^{\mathrm{LUMO}} &= \frac{\partial E^{\mathrm{KS}}(\mathrm{LUMO})}{\partial \delta n} \\ U_0^{\mathrm{HOMO}} &= \frac{\partial E^{\mathrm{KS}}(\mathrm{HOMO})}{\partial \delta n} \end{aligned} \quad (3)$$

relate the change in the molecular levels with respect to their occupation numbers, δn, to the charging energies.

When the molecule is interacting with a metal surface, image potential effects at the M/O interface induce on the metal side an opposite charge to the one appearing on the molecule, shifting the empty and filled molecular levels in opposite directions and reducing the value of the transport gap [33,43–45] to:

$$E^t = E^{\mathrm{KS}} + \frac{U_0^{\mathrm{LUMO}} + U_0^{\mathrm{HOMO}}}{2} - V^{im} = E^{\mathrm{KS}} + U = E^t(gas) - V^{im} \quad (4)$$

where the effective charging energy $U_0 = (U_0^{\mathrm{LUMO}} + U_0^{\mathrm{HOMO}})/2$ has been reduced to $U = (U_0^{\mathrm{LUMO}} + U_0^{\mathrm{HOMO}})/2 - V^{im} = U_0 - V^{im}$.

In our approach, we correct the transport energy gap using Eq. (4). The basic idea is to perform DFT–LDA calculations to determine V^{im}, and then use an accurate calculation of $E^t(gas)$ to obtain the transport energy gap of the molecule on the surface, E^t. The value of $E^t(gas)$ can be obtained from experiment or from accurate theoretical calculations. In the present case we use the value from the OCTOPUS calculation mentioned above, $E^t(gas) = 6.3$ eV. V^{im} is calculated as the difference between the charging energy of the molecule on the surface, U, and the charging energy of the gas-phase molecule, both calculated with the FIREBALL code.

As discussed in Refs. [33–35], U can be related to the potential induced in the molecule, V^{IDIS} (see below), and to the number of electrons transferred to/from it, δn, by the equation $U = e\partial V^{\mathrm{IDIS}}/\partial\delta n \cong eV^{\mathrm{IDIS}}/\delta n$. This equation can be seen as a generalization of Eq. (3) for the HOMO and LUMO levels: in practice (see below) due to the charge transfer, the molecule DOS around the HOMO and LUMO levels is shifted rigidly by V^{IDIS}. V^{IDIS}, δn and $e\partial V^{\mathrm{IDIS}}/\partial\delta n$ are obtained from our DFT–LDA FIREBALL calculations, yielding $U(FB) = 2.95$ eV and V^{im}=$U^0(FB) - U(FB)$=1.94 eV for the geometry shown in Fig. 2B. We stress that, in order to determine U and V^{im}, we have analyzed the case of an isolated molecule on the surface (see Fig. 1A), the reason being that the effect of the other neighboring molecules on V^{im} is small because of the larger screening of the metal. Therefore, this same value of U is used for the other adlayer cases.

Once we have determined V^{im}, the correct E^t is introduced in our FIREBALL Kohn–Sham Hamiltonian by means of a scissor operator:

$$\mathbf{O}^{scissor} = U/2\sum_{\mu_i,v_i}\{|\mu_i\rangle\langle\mu_i| - |v_i\rangle\langle v_i|\} \tag{5}$$

$|\mu_i\rangle$ ($|v_i\rangle$) being the empty (occupied) orbitals of the isolated molecule (with the actual geometry of the molecule on the surface) [33]. Notice that while the shift operator O^{shift} (see Section 2) moves rigidly all the levels of the molecule with respect to the metal, the scissor operator $O^{scissor}$ moves filled and empty molecular states in opposite directions, changing the value of the gap E^t. Obviously U depends on E^t, and this forces us to calculate E^t and U selfconsistently. We also use $\mathbf{O}^{scissor}$ to correct the error in the LDA gap due to the non-converged basis set used in our calculations.

3. Tunneling currents, STM imaging and geometry

3.1. Tunneling currents and STM images

Fig. 2A shows three different TTF/Au (1 1 1) adsorption geometries obtained using different standard DFT simulation packages. Configuration I corresponds to a relaxed structure obtained using the VASP code [46,47], with the LDA exchange–correlation (XC) functional and a plane-wave cutoff of 286 eV, while configurations II and III correspond to relaxed structures obtained using the DACAPO code [48], with the GGA-revPBE XC functional and a plane-wave cutoff of 400 eV, and the GAUSSIAN03 code [49], at B3LYP/6-31+G* level, respectively. These structures are quite different; in order to elucidate which one corresponds to the actual adsorption geometry we have calculated the theoretical STM images (as explained below) and compared them with the experimental one [22], shown in Fig. 2B. In the three cases we find that the theoretical STM image does not agree with the experimental one, suggesting that for this weakly interacting case LDA or GGA calculations do not describe properly the molecule/surface adsorption geometry, probably due to the lack of van der Waals forces in these calculations (for a treatment of van der Waals forces within DFT see Refs. [50–55]).

Thus, we have explored the TTF/Au (1 1 1) adsorption geometry by performing accurate theoretical simulations for the STM-image for different adsorption geometries (more than 200) where the orientation, the adsorption position and distance of the molecule relative to the surface, as well as the internal geometry of the molecule, have been changed. Then, we look for the configuration yielding the best agreement with the available experimental evidence [22]. In our approach, tunneling currents for the STM images have been calculated using a Keldysh–Green function formalism together with the first-principles tight-binding Hamiltonian obtained from the local-orbital DFT-FIREBALL method (as explained in detail elsewhere [39,56]). Some examples of the application of this approach can be found in references [32,57,58]; in particular, reference [57] is a good example of how the accurate theoretical simulation of STM images, and its comparison with high-quality experimental STM images, can guide us towards the correct atomic structure. In the following we present a brief description of this formalism.

In the theoretical STM simulations, we rewrite the total tip-sample Hamiltonian describing the system as H_{T}, H_{S} and T_{TS}, where the total system is split into two parts, T (tip) and S (sample: molecule/Au surface), T_{TS} defining the coupling between both. In the present case we have assumed to have a tip formed by five atoms, one of them in the apex, joined to four layers of W (1 0 0). Then, the equation for the current I is given by [39,56]:

$$I = \frac{4\pi e^2}{h}\int_{E_F}^{E_F+eV}\mathrm{Tr}[T_{\mathrm{TS}}\rho_{\mathrm{SS}}(\omega)D^r_{\mathrm{SS}}(\omega)T_{\mathrm{ST}}\rho_{\mathrm{TT}}(\omega - eV)D^a_{\mathrm{TT}}(\omega - eV)]d\omega \tag{6}$$

where $D^r_{\mathrm{SS}} = [1 - T_{\mathrm{ST}}g^r_{\mathrm{TT}}T_{\mathrm{TS}}g^r_{\mathrm{SS}}]^{-1}$, and $D^a_{\mathrm{TT}} = [1 - T_{\mathrm{TS}}g^a_{\mathrm{SS}}T_{\mathrm{ST}}g^a_{\mathrm{TT}}]^{-1}$; $g^{r(a)}_{\mathrm{TT}}$ and $g^{r(a)}_{\mathrm{SS}}$ are the retarded (advanced) Green functions of the decoupled tip and surface subsystems, ρ_{TT} and ρ_{SS} are the density of states matrices, where $\rho_{ij} = \pm\frac{1}{\pi}\Im g^{a/r}_{ij}$; and V the tip–sample applied bias. Notice that Eq. (6) is only valid for 0 K temperature; occupation distribution functions should be included for a finite temperature value.

In this approach the W-tip and the sample (TTF/Au (1 1 1)) are calculated independently providing g^r_{TT} and g^r_{SS}; then, T_{TS} is calculated using a dimer approximation: a dimer formed by one W-atom (corresponding to the tip) and another surface one (S, C, H or Au coming from the sample) is calculated for different atom–atom distances and for all the non-zero interactions. The details are explained in Ref. [39,56].

In the tunneling regime D^a_{TT} and D^r_{SS} can be approximated by the unit matrix, so Eq. (6) turns to:

$$I \cong \frac{4\pi e^2}{h}\int_{E_F}^{E_F+eV}\mathrm{Tr}[T_{\mathrm{TS}}\rho_{\mathrm{SS}}(\omega)T_{\mathrm{ST}}\rho_{\mathrm{TT}}(\omega - eV)]d\omega \tag{7}$$

Using this equation for the tunneling current, we have calculated STM images for different adsorption geometries of TTF on Au (1 1 1) as explained in the following section.

3.2. Geometry

As mentioned above, we have used this theoretical STM tool to look for the adsorption geometry of TTF on Au (1 1 1). For this purpose, we compare our theoretical STM images with the experimental image, and analyze how the changes in adsorption geometry change the theoretical STM image. In total we have explored more than 200 different geometries. Fig. 2 (bottom-right) shows the one found yielding the best agreement with the experimental image (see top-right image). In this geometry, the molecule is rather flat, being located at 3.05 Å from the surface. A side view of the theoretically STM-engineered structure is also shown in Fig. 2. In this simulations, W-tip height from TTF monolayer and surface voltage, V_s, take the values of 4.5 Å and −1 eV, respectively, in order to mimic the experimental STM signal [22]. It is worth stressing that the variation of the W-tip height between 4 and 5 Å does not reveal any significant change in the theoretical STM signal. These theoretical STM images have been calculated with FIREBALL taking into account the different corrections already discussed for the TTF/Au (1 1 1) electronic structure.

In order to give a flavor of the different geometries analyzed to obtain the geometry shown in Fig. 2, we show in Fig. 3 a few intermediate representative cases with their corresponding STM-images. Case A corresponds to an ideal, undeformed, TTF molecule located parallel to the Au (1 1 1) surface; in this case, the STM-image represents two lobes which are far from the experimental image [22]. Case B corresponds to the geometry calculated using DACAPO (see Fig. 2, too); the visible assymmetry of the molecule, associated with the bonding of the double C-bond with the surface, introduces a similar assymmetry in the STM-image. Case C shows a critical deformation of the S atoms, with the S–C–S angle larger than in the ideal geometry: this deformation introduces the four bright spots shown in the STM-image associated with the S atoms. Case D, the final geometry, is obtained by moving the right double C-bond towards its initial position, the S atoms slightly upwards (around 0.2 Å higher than the C atoms) and, at the same time, closing a little the left double C-bond; obviously, all these small displacements have been deeply analyzed with many other intermediate geometries.

We also show in Fig. 3, for the sake of completeness, three additional cases, D′, D″; and D‴, where the molecule of case D has been displaced 0.2 Å upwards and downwards the surface (cases D′ and D″, respectively) or 0.1 Å parallel to the surface (case D‴); the corresponding STM images indicate how the theoretical STM-imaging depends on the position of the molecule on the Au surface. Although determining the adsorption distance from a comparison of theoretical and experimental STM images is a challenging problem, images calculated by displacing the molecule outwards/downwards suggest that the molecule-surface distance is determined within an error bar of ±0.1 Å. We have also tilted the molecule 3°, with two of the lateral S atoms higher than the other two, and have found that the STM-image is much worse than the one given in Fig. 3D; this indicates that the molecule is almost flat, with a very slight tilting.

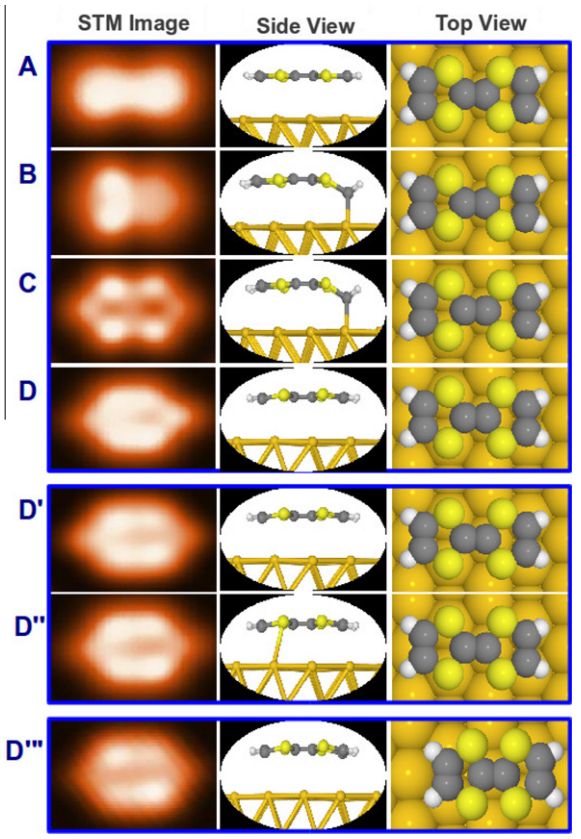

Fig. 3. Theoretical STM images of TTF on Au (1 1 1) surface for some representative intermediate configurations (explained in the text); top and side view for each structure is also shown.

4. Interface properties

Once we have obtained the interface geometry, we calculate the interface electronic properties of: (a) the single molecule; and (b) the other TTF-layers, as well as the corresponding charging energy effects. The single molecule case allows us to determine U as explained above, while the other cases can be related to a kind of effective U [59]:

$$U^{eff} = \frac{eV^{\mathrm{IDIS}}}{\delta n} = U + \sum J_i \tag{8}$$

where J_i is the effective intersite coulomb interaction between charges in different molecules This is a pure electrostatic effect that is not related with the correlation effects involved in self-interaction correction and image potential. Thus, J_i does not change the transport gap so $E^t = E^{KS} + U$ for all interfaces.

4.1. TTF molecule on Au (1 1 1)

Fig. 4 shows the electron DOS projected on the TTF orbitals for the case of a single molecule adsorbed on Au (1 1 1) (Fig. 1A). In the same figure we also show the molecule energy levels of the isolated (but deformed) molecule; the energy window around the energy gap is enlarged in the inset. In this figure the molecule transport gap has been

corrected as discussed in Section 3; for comparison, the levels for the isolated molecule are corrected using the same value of U as in the case of the molecule on the Au (1 1 1) surface. The initial Fermi level, Φ_M (whose absolute value defines the Au work function: 5.3 eV), the interface Fermi energy, E_F (this is the metal Fermi level after the contact is established), the HOMO and LUMO levels, as well as the *CNL*, are shown. This last quantity is calculated integrating the molecule DOS up to the number of electrons of the neutral molecule. The main effect of the contact is to broaden the molecular levels, creating an induced density of interface states, and to shift the metal Fermi level from Φ_M to E_F.

As in a typical MO interface, the TTF/Au contact creates an induced density of interface states in the molecule and thus a charge transfer between molecule and metal. This gives rise to a potential, V^{IDIS}, between the molecule and the metal that tries to align the initial metal Fermi level Φ_M and the organic *CNL* [14,18]. This pinning is governed by the screening parameter S defined as:

$$(CNL - E_F) = S(CNL - \Phi_M) \tag{9}$$

notice that $0 < S < 1$, with $S \to 0$ or 1 for high or low screening, respectively [34]. In the limit of large screening the *CNL* and E_F tend to be aligned, while for $S \to 1$, we recover the Schottky–Mott limit with no interface IDIS-potential. On the other hand:

$$eV^{\mathrm{IDIS}} = (E_F - \Phi_M) = (1 - S)(CNL - \Phi_M) \tag{10}$$

We have checked, by changing in our calculations Φ_M fictitiously (see Fig. 5), that the value of S is practically constant in a moderate range of Φ_M values: for the isolated TTF molecule on Au (1 1 1) we obtain $S = 0.66$.

We can also relate S to some general interface quantities. To this end, consider the equation (see Section 2):

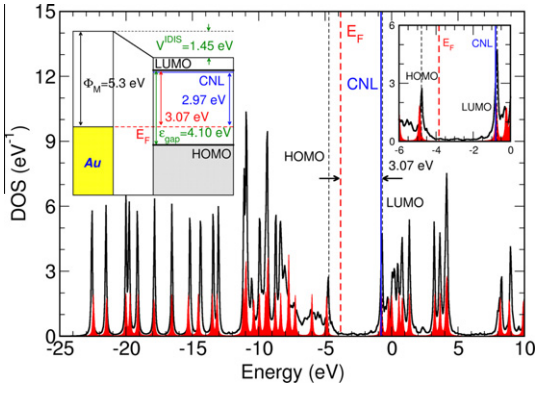

Fig. 4. DOS profile for a single TTF molecule on Au (1 1 1) (cluster model; see Fig. 1); the initial molecular levels are shown by the red shaded region (with a broadening of $\eta = 0.05$ eV). Fermi, HOMO and LUMO levels are also indicated on the figure. The left inset shows an energy diagram for the system. The molecule transport gap has been corrected as discussed in Section 3; for comparison, the levels for the isolated molecule are corrected using the same value of U as in the case of the molecule on the Au (1 1 1) surface. In the DOS profiles the vacuum level for the adsorbed molecule is kept aligned to the vacuum level for the isolated molecule. (For interpretation of the references to color in this figure legend, the reader is referred to the web version of this paper.)

$$U = \frac{eV^{\mathrm{IDIS}}}{\delta n} = \frac{(1 - S)(CNL - \Phi_M)}{\delta n} \tag{11}$$

Then we define a mean density of states (spin included) between *CNL* and E_F, $\widetilde{D}$, so that δn is given by:

$$\delta n = \widetilde{D}(CNL - E_F) \tag{12}$$

Combining Eqs. (10)–(12), it can be easily found:

$$S = \frac{1}{1 + U\widetilde{D}} \tag{13}$$

in this equation, $U\widetilde{D}$ plays the same role that the term $4\pi e^2 d\widetilde{D}/A$ does in the elementary theory of Schottky barriers (d is the effective distance between the positive and negative charge transferred between the metal and the molecule, and A the area per molecule). Both Eqs. (11) or (13) can be used to obtain the molecule charging energy: our calculations yield $U_{FB} = 2.95$ eV (see Section 3 and also the Appendix). As mentioned above, this indicates that in our FIREBALL calculations, image potential effects reduce the energy gap by 1.94 eV. This yields (see Eq. (4)) E^t = 6.3–1.94 = 4.36 eV; the deformation of the molecule also reduces slightly E^t to a final value of 4.1 eV (see Figs. 4, 6 and 7). Finally, we comment that for this case we obtain a charge transfer of 0.43 electrons (see Fig. 5), and a surface dipole, D, of 6.3 Debyes.

4.2. Monolayer (HB) and fraction of monolayer cases

Fig. 7 shows the molecule local DOS for the HB-geometry (the monolayer case); we show here the same quantities as in Fig. 4: Φ_M, E_F, the *CNL* and the HOMO and LUMO levels. As in the previous case, we also see how the quantity $(CNL - \Phi_M)$, has been screened to $(CNL - E_F)$, so that Eq. (9) is also valid for the monolayer case, but with a different screening parameter, $S = 0.47$ in this case. It is interesting to realize that this parameter, S, is now significantly smaller than in the case of the single molecule on the surface

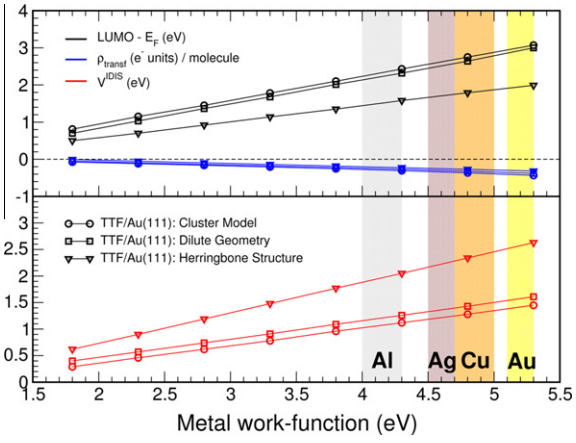

Fig. 5. (LUMO – E_F) and transfer of charge (upper panel), and V^{IDIS} (lower panel) as a function of the metal work-function. This figure tries to simulate how the interface properties depend on the initial Fermi level of different metals: this issue is shown in the figure by superimposing the initial Fermi levels (that is the metal work function with a negative sign) of Al, Ag, Cu and Au for comparison.

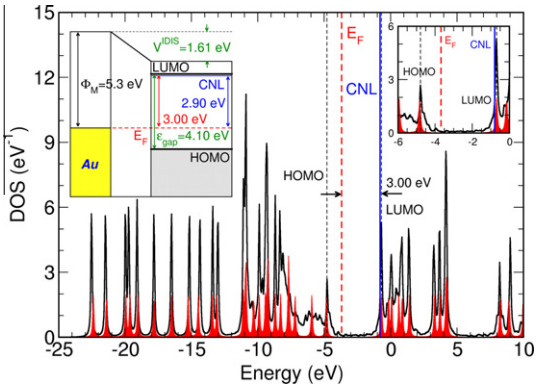

Fig. 6. DOS profile for the TTF molecule on Au (111) (dilute geometry; see Fig. 1); the initial molecular levels are shown by the red shaded region (with a broadening of $\eta = 0.05$ eV). Fermi, HOMO and LUMO levels are also indicated on the figure. The left inset shows an energy diagram for the system. The molecule transport gap has been corrected as discussed in Section 3; for comparison, the levels for the isolated molecule are corrected using the same value of U as in the case of the molecule on the Au (111) surface. In the DOS profiles the vacuum level for the adsorbed molecules is kept aligned to the vacuum level for the isolated molecule.

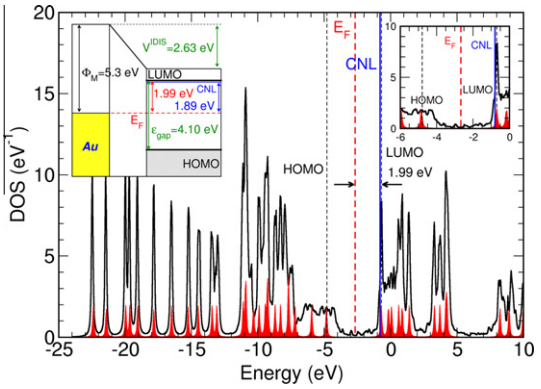

Fig. 7. DOS profile for the TTF monolayer on Au (111) (herringbone structure; see Fig. 1); the initial molecular levels are shown by the red shaded region (with a broadening of $\eta = 0.05$ eV). Fermi, HOMO and LUMO levels are also indicated on the figure. The left inset shows an energy diagram for the system. The molecule transport gap has been corrected as discussed in Section 3; for comparison, the levels for the isolated molecule are corrected using the same value of U as in the case of the molecule on the Au (111) surface. In the DOS profiles the vacuum level for the adsorbed molecules is kept aligned to the vacuum level for the isolated molecule.

($S = 0.66$), reflecting a larger screening effect. For the 6×6-geometry (see Fig. 6) we find an interface behaviour similar to the single molecule case, indicating that for this dilute periodic structure the molecule–molecule interaction is very small. As in the single molecule case, we have changed in our DFT-calculations Φ_M fictitiously, and found that S is constant for moderate changes (see Fig. 4).

In Figs. 6 and 7 we have also shown the IDIS potential, V^{IDIS}, induced in the molecule by the MO-charge transfer; in our calculations, this charge transfer per molecule is 0.37 and 0.31 electrons for the 6×6-geometry and the HB-structure, respectively, with the corresponding surface dipoles, D, of 5.4 (6×6) and 4.5 (HB) Debyes, and $V^{\mathrm{IDIS}} = 1.61$ (6×6) and 2.63 (HB) eV. Notice that this IDIS potential is different from the electrostatic potential, $V^{av} = 4\pi e^2 d\delta n/A$, created between the metal and vacuum (A is the area per molecule): for dilute geometries, V^{av} is smaller than V^{IDIS}, while for the compact HB-monolayer, $V^{av} \simeq V^{\mathrm{IDIS}}$. In our results we find that the TTF–*CNL* is located around 0.1 eV from the LUMO level of the interacting molecule, namely, 0.8 eV from vacuum, which corresponds – as expected – to a case having a strong donor character.

We can also relate S to U^{eff}, defined for the adlayer case as $U^{eff} = eV^{\mathrm{IDIS}}/\delta n$, by replacing U by U^{eff} in Eqs. (11) and (13); this yields:

$$S = 1/(1 + U^{eff}\widetilde{D}) \tag{14}$$

Notice that for these cases V^{IDIS} depends also on the interaction between molecules; therefore U^{eff} contains both intramolecular (U) and intermolecular (J_i) contributions [59], see Eq. (8). From our calculations we obtain U^{eff}=3.6 and 6.7 eV for the (6×6) and herringbone cases, respectively. Finally, we mention that in these cases the corrections related to the "pillow" dipole [34] are small, see Appendix.

5. Discussion and conclusions

Other theoretical calculations for the TTF/Au (111) interface have already been reported by Fernández-Torrente et al. [22] and Hofmann et al. [24] where 6×4 and 6×5 unit cells have been considered, respectively. In both studies a GGA-DFT code has been used, although it has been mentioned [24] that probably "the actual equilibrium distance between the organic adsorbate and the metal surface lies in between the two extreme cases provided by GGA and LDA formalisms".

In our approach we took advantage of looking for the best TTF geometry, by comparing the experimental STM images reported in Ref. [22] with the theoretical ones calculated for more than 200 geometries. The geometry obtained in this way is shown in Fig. 2; the calculated STM-image for the best candidate fits considerably well with the experimental one and improves a lot the images calculated for the geometries provided by conventional LDA or GGA calculations. That new geometry is rather flat, parallel to the Au-surface, and located at 3.05 Å from it.

TTF has a strong donor character, which is shown in the present study by the position of the *CNL* for all the considered system models, located at 0.8 eV below the molecule vacuum, and by the electron charge transfer from TTF to Au, which for the single molecule is 0.43 electrons, and 0.37 and 0.31 electrons for the 6×6 and HB structures, respectively. Our calculations yield induced dipoles per molecule of 6.3 (single molecule), 5.4 (6×6 geometry) and 4.5 (HB structure) Debyes. It is interesting to remark that these values do not differ significantly from those found by Fernández-Torrente et al. [22]: 5 Debyes for a 6×4 unit cell, and Hofmann et al. [24]: 4.5 Debyes for a $5 \times 3\sqrt{3}$ unit cell, showing that the charge transfer mechanism is not altered too much by the molecule geometries. Recent experimental data from Ref. [60] yields a molecular dipole of 5.4 Debyes for very low coverages, in excellent

agreement with our results; however, the values for higher coverages ($\theta \geqslant 0.5$) cannot be directly compared with our results because of the interface inhomogeneities, due to island formation.

In our approach we have also addressed the issue of the organic energy gap problem, calculating the molecule charging energy U and using Eq. (4) to obtain E^t. We find that surface polarization effects reduced the gas-phase molecule transport energy gap by 1.9 eV; this value corresponds to an effective distance of 3.8 Å between the TTF induced charge and its image (notice that the molecule size is around 7 Å). The deformation of the molecule on the surface also reduces slightly E^t (by ~ 0.25 eV), and we finally obtain $E^t = 4.1$ eV for TTF on Au (1 1 1). DFT-GGA calculations [22] yield a much smaller energy gap and therefore very different barrier heights for electrons or holes. We also find that the amount of charge transferred from TTF to Au (1 1 1) does not seem to depend too much on the value of E^t.

In conclusion, we have presented, by using a DFT approach, a discussion of the TTF/Au (1 1 1) interface properties. For this purpose, firstly we have analyzed the geometry of the molecule on the Au surface using a fitting to the experimental STM image. We propose this theoretical STM-engineering technique as a powerful tool to elucidate ground-state configurations for those systems which may be geometrical and electronically poorly described by the standard DFT tools. In a second step, we have also discussed, based on the final STM-engineered TTF/Au structure, the interface dipole and the barrier height formation, including charging energy effects in the molecule energy gap. Our results show that the interface dipole, as calculated in the present DFT approach, is mainly due to the organic–metal charge transfer and the induced density of interface states associated with the metal–organic interaction, a mechanism already described by the IDIS model. We also provide the molecule CNL that we find at 0.8 eV from vacuum, as corresponds to the high donor character of TTF.

Acknowledgements

This work is supported by Spanish MICIIN under contracts MAT2007-60966 and FIS2010-16046, the CAM under contract S2009/MAT-1467 and the European Project MINOTOR (Grant FP7-NMP-228424). E.A. gratefully acknowledges financial support by the Consejería de Educación of the CAM, the FSE and the European Project MINOTOR. J.I.M. acknowledges funding from Spanish MICIIN through Juan de la Cierva Program. C.G. acknowledges the CSIC post-doc JAE contract and the Spanish MICIIN projects MAT2008-01497 and CSD2007-00041.

Appendix A

In this Appendix we comment some technical issues regarding our FIREBALL calculations. In FIREBALL the Hartree potential is calculated by approximating, in a selfconsistent fashion, the total charge by a superposition of spherical charges around each atom. This approximation neglects off-diagonal contributions of the induced charge (dipolar contributions) whose effects, although not important for the selfconsistent calculation itself, introduces non-negligible contributions to the induced Hartree potential. One of these effects is related to the induced "pillow" dipole [34], which is created by the compression of the electron metal tails due to their overlap with the organic molecule wavefunctions. The second effect we consider here is associated with the charge induced on the metal surface and the accompanying induced "metal surface" dipole that tends to shift that surface charge from practically the last metal layer to the image plane located outwards. These two effects are introduced as perturbations in our calculations [34].

The "pillow" dipole corrections are calculated as detailed in Ref. [34]. A deep analysis of this dipole contribution can be associated with the overlap between the metal/organic wave functions. This correction can be introduced in our calculations as follows [14]:

$$eV^t = eV^{\mathrm{IDIS}} + eV^{\mathrm{pillow}} \quad \text{where } eV^{\mathrm{pillow}} = SeV_0^{\mathrm{pillow}} \tag{15}$$

In our case $eV_0^{\mathrm{pillow}} = 0.10$, 0.04 and 0.04 eV; so $eV^{\mathrm{pillow}} = SeV_0^{\mathrm{pillow}} = 0.05, 0.03$ and 0.03 eV for the HB, dilute and molecular cases, respectively.

The induced "metal surface" dipole is calculated by means of the off-diagonal induced charge:

$$en_{ij} = -\frac{e}{\pi}\int \Im G_{ij}(\omega)d\omega \tag{16}$$

$G_{ij}(\omega)$ being the Green function of our system, defined by the local-orbital Hamiltonian, as obtained from our DFT calculation in the local orbital basis. From en_{ij} we calculate straightforwardly the corresponding induced Hartree potential. The induced "metal-surface" dipole [34], is a part of the IDIS dipole associated with the off-diagonal terms of the induced "metal-surface" charge (neglected in the Hartree potential). The calculation of the potential created by these induced off-diagonal charges changes V^{IDIS} by −0.24, −0.12 and −0.12 for the HB, dilute and molecular cases, respectively; this also reduces U_{FB} by 0.25 eV to the final value 2.95 eV given above.

It is also important to discuss the issue of the convergence of our calculations with the basis set. In this direction, we have analyzed how our results depend on having a more extended basis set; in particular, we have used the following one: $sp^3d^5s^*d^{*5}$ NAOs for Au, sp^3d^5 for C and S, and ss^* for H, with the following cut-off radii (in a.u.): $s = 6.0$. $p = 7.0$, $d = 5.0$, $s^* = 6.0$ and $d^* = 5.0$ (Au); $s = 4.0$. $p = 4.5$, $d = 5.4$ (C); $s = 4.2$. $p = 4.7$, $d = 5.5$ (S); and $s = 4.5$ and $s^* = 4.5$ (H). Using this more complete basis set shifts the molecular levels, but the "scissor" and "shift" operators discussed above allow us to fit the molecule energy gap and its energy position to the experimental values. We find that using these corrections, our calculation of the interface dipole and the charging energy is well converged in our original basis set calculation. The exception to this result is the calculation of the "pillow" dipole, which is substantially increased in the more extended basis. In particular, the "pillow" dipole, SeV_0^p, of 0.05 eV found (for the HB structure) with the minimal basis set is

increased to 0.30 eV for the extended basis, and to 0.12 eV for the isolated molecule and the 6×6 structure. Notice that these values of SeV_0^p compensate very accurately the changes in V^{IDIS} associated with the "metal-surface" dipole.

References

[1] W.R. Salanek, S. Stafstrom, J.L. Bredas, Conjugated Polymer Surfaces and Interfaces: Electronic and Chemical Structure of Interfaces for Polymer Light Emitting Diodes, Cambridge University Press, 1996.

[2] N. Koch, Organic electronic devices and their functional interfaces, ChemPhysChem 8 (2007) 1438–1455.

[3] C. Shen, A. Kahn, The role of interface states in controlling the electronic structure of Alq3/reactive metal contacts, Org. Electron. 2 (2001) 89–95.

[4] D. Cahen, A. Kahn, E. Umbach, Energetics of molecular interfaces, Mater. Today 8 (2005) 32–41.

[5] H. Ishii, K. Sugiyama, E. Ito, K. Seki, Energy level alignment and interfacial electronic structures at organic/metal and organic/organic interfaces, Adv. Mater. 11 (1999) 605–625.

[6] S. Narioka, H. Ishii, D. Yoshimura, M. Sei, Y. Ouchi, K. Seki, S. Hasegawa, T. Miyazaki, Y. Harima, K. Yamashita, The electronic structure and energy level alignment of porphyrin/metal interfaces studied by ultraviolet photoelectron spectroscopy, Appl. Phys. Lett. 67 (1995) 1899.

[7] I.G. Hill, A. Rajagopal, A. Kahn, Y. Hu, Molecular level alignment at organic semiconductor–metal interfaces, Appl. Phys. Lett. 73 (1998) 662.

[8] I.G. Hill, J. Schwartz, A. Kahn, Metal-dependent charge transfer and chemical interaction at interfaces between 3,4,9,10-perylenetetracarboxylic bisimidazole and gold, silver and magnesium, Org. Electron. 1 (2000) 5–13.

[9] X. Crispin, V. Geskin, A. Crispin, J. Cornil, R. Lazzaroni, W.R. Salaneck, J.L. Brédas, Characterization of the interface dipole at organic/metal interfaces, J. Am. Chem. Soc. 124 (2002) 8131–8141.

[10] M. Knupfer, G. Paasch, Origin of the interface dipole at interfaces between undoped organic semiconductors and metals, J. Vac. Sci. Technol. A 23 (2005) 1072.

[11] S. Yanagisawa, Y. Morikawa, Theoretical investigation of the electronic structure of the Alq3/Mg interface, J. Phys. Condens. Matter 21 (2009) 64247.

[12] P. Bagus, V. Staemmler, C. Wöll, Exchange-like effects for closed-shell adsorbates: interface dipole and work function, Phys. Rev. Lett. 89 (2002) 96104.

[13] G. Witte, S. Lukas, P.S. Bagus, C. Wöll, Vacuum level alignment at organic/metal junctions: cushion effect and the interface dipole, Appl. Phys. Lett. 87 (2005) 263502.

[14] H. Vázquez, Y.J. Dappe, J. Ortega, F. Flores, Energy level alignment at metal/organic semiconductor interfaces: "pillow" effect, induced density of interface states, and charge neutrality level, J. Chem. Phys. 126 (2007) 144703.

[15] H. Vázquez, R. Oszwaldowski, P. Pou, J. Ortega, R. Pérez, F. Flores, A. Kahn, Dipole formation at metal/PTCDA interfaces: role of the charge neutrality level, Europhys. Lett. 65 (2004) 802–808.

[16] H. Vázquez, F. Flores, R. Oszwaldowski, J. Ortega, R. Pérez, A. Kahn, Barrier formation at metal/organic interfaces: dipole formation and the charge neutrality level, Appl. Surf. Sci. 234 (2004) 107–112.

[17] M. Betti, A. Kanjilal, C. Mariani, H. Vázquez, Y. Dappe, J. Ortega, F. Flores, Barrier formation at organic interfaces in a Cu(100)-benzenethiolate–pentacene heterostructure, Phys. Rev. Lett. 100 (2008) 27601.

[18] F. Flores, J. Ortega, H. Vázquez, Modelling energy level alignment at organic interfaces and density functional theory, PhysChemChemPhys 11 (2009) 8658–8675.

[19] S. Braun, W.R. Salaneck, M. Fahlman, Energy-level alignment at organic/metal and organic/organic interfaces, Adv. Mater. 21 (2009) 1450–1472.

[20] J. Hwang, A. Wan, A. Kahn, Energetics of metal–organic interfaces: new experiments and assessment of the field, Mater. Sci. Eng. R 64 (2009) 1–31.

[21] S. Kümmel, L. Kronik, Orbital-dependent density functionals: theory and applications, Rev. Mod. Phys. 80 (2008) 3–60.

[22] I. Fernández-Torrente, S. Monturet, K. Franke, J. Fraxedas, N. Lorente, J. Pascual, Long-range repulsive interaction between molecules on a metal surface induced by charge transfer, Phys. Rev. Lett. 99 (2007) 176103.

[23] H. Yan, S. Li, C. Yan, Q. Chen, L. Wan, Adsorption of TTF, TCNQ and TTF–TCNQ on Au (111): an in situ ECSTM study, Sci. China Ser. B Chem. 52 (2009) 559–565.

[24] O.T. Hofmann, G.M. Rangger, E. Zojer, Reducing the metal work function beyond pauli pushback: a computational investigation of tetrathiafulvalene and viologen on coinage metal surfaces, J. Phys. Chem. C 112 (2008) 20357–20365.

[25] H.J. Monkhorst, J.D. Pack, Special points for Brillouin-zone integrations, Phys. Rev. B 13 (1976) 5188–5192.

[26] J.P. Lewis, P. Jelínek, J. Ortega, A.a. Demkov, D.G. Trabada, B. Haycock, H. Wang, G. Adams, J.K. Tomfohr, E. Abad, H. Wang, D.a. Drabold, Advances and applications in the FIREBALL ab-initio tight-binding molecular-dynamics formalism, Phys. Stat. Sol. B 248 (2011) 1989–2007.

[27] J. Lewis, K. Glaesemann, G. Voth, J. Fritsch, A. Demkov, J. Ortega, O. Sankey, Further developments in the local-orbital density-functional-theory tight-binding method, Phys. Rev. B 64 (2001) 195103.

[28] P. Jelínek, H. Wang, J. Lewis, O. Sankey, J. Ortega, Multicenter approach to the exchange–correlation interactions in ab-initio tight-binding methods, Phys. Rev. B 71 (2005) 235101.

[29] O. Sankey, D. Niklewski, Ab-initio multicenter tight-binding model for molecular-dynamics simulations and other applications in covalent systems, Phys. Rev. B 40 (1989) 3979–3995.

[30] M. Basanta, Y. Dappe, P. Jelínek, J. Ortega, Optimized atomic-like orbitals for first-principles tight-binding molecular dynamics, Comput. Mater. Sci. 39 (2007) 759–766.

[31] M. Fuchs, M. Scheffler, Ab-initio pseudopotentials for electronic structure calculations of polyatomic systems using density-functional theory, Comput. Phys. Commun. 119 (1999) 67–98.

[32] J.I. Martínez, E. Abad, F. Flores, J. Ortega, Simulating the organic-molecule/metal interface: TCNQ/Au(111), Phys. Stat. Sol. B 248 (2011) 2044–2049.

[33] E. Abad, C. González, J. Ortega, F. Flores, Charging energy, self-interaction correction and transport energy gap for a nanogap organic molecular junction, Org. Electron. 11 (2010) 332–337.

[34] E. Abad, Y.J. Dappe, J.I. Martínez, F. Flores, J. Ortega, C_6H_6/Au(111): interface dipoles, band alignment, charging energy, and van der Waals interaction, J. Chem. Phys. 134 (2011) 044701.

[35] E. Abad, J.I. Martínez, J. Ortega, F. Flores, Barrier formation and charging energy for a variable nanogap organic molecular junction: a tip/C_{60}/Au(111) configuration, J. Phys. Condens. Matter 22 (2010) 304007.

[36] A. Demkov, J. Ortega, O. Sankey, M. Grumbach, Electronic structure approach for complex silicas, Phys. Rev. B 52 (1995) 1618–1630.

[37] J. Harris, Simplified method for calculating the energy of weakly interacting fragments, Phys. Rev. B 31 (1985) 1770–1779.

[38] W. Foulkes, R. Haydock, Tight-binding models and density-functional theory, Phys. Rev. B 39 (1989) 12520–12536.

[39] J.M. Blanco, F. Flores, R. Perez, STM-theory: image potential, chemistry and surface relaxation, Prog. Surf. Sci. 81 (2006) 403–443.

[40] M.A.L. Marques, A. Castro, G.F. Bertsch, A. Rubio, OCTOPUS: a first-principles tool for excited electron–ion dynamics, Comput. Phys. Commun. 151 (2003) 60–78.

[41] C. Adamo, G.E. Scuseria, V. Barone, Accurate excitation energies from time-dependent density-functional theory: assessing the PBE0 model, J. Chem. Phys. 111 (1999) 2889.

[42] J. Janak, Proof that $\partial E/\partial n_i = \epsilon_i$ in density-functional theory, Phys. Rev. B 18 (1978) 7165–7168.

[43] J. Sau, J. Neaton, H. Choi, S. Louie, M. Cohen, Electronic energy levels of weakly coupled nanostructures: C_{60}/metal interfaces, Phys. Rev. Lett. 101 (2008) 26804.

[44] J. Neaton, M. Hybertsen, S. Louie, Renormalization of molecular electronic levels at metal/molecule interfaces, Phys. Rev. Lett. 97 (2006) 216405.

[45] J.M. García-Lastra, C. Rostgaard, A. Rubio, K.S. Thygesen, Polarization-induced renormalization of molecular levels at metallic and semiconducting surfaces, Phys. Rev. B 80 (2009) 245427.

[46] G. Kresse, J. Furthmüller, Efficient iterative schemes for ab-initio total-energy calculations using a plane-wave basis set, Phys. Rev. B 54 (1996) 11169–11186.

[47] Vienna Ab-initio Simulation Package. Available from: <http://cms.mpi.univie.ac.at/vasp/>.

[48] B. Hammer, L. Hansen, J. Nørskov, Improved adsorption energetics within density-functional theory using revised Perdew–Burke–Ernzerhof functionals, Phys. Rev. B 59 (1999) 7413–7421.

[49] M.J. Frisch et al., Gaussian 03, Gaussian, Inc., Wallingford, CT, 2004. Available from: <http://www.gaussian.com>.

[50] J. Ángyán, I. Gerber, A. Savin, J. Toulouse, Van der Waals forces in density functional theory: perturbational long-range electron-interaction corrections, Phys. Rev. A 72 (2005) 12510.
[51] D.C. Langreth, M. Dion, H. Rydberg, E. Schröder, P. Hyldgaard, B.I. Lundqvist, Van der Waals density functional theory with applications, Int. J. Quantum Chem. 101 (2005) 599–610.
[52] F. Ortmann, F. Bechstedt, W. Schmidt, Semiempirical Van der Waals correction to the density-functional description of solids and molecular structures, Phys. Rev. B 73 (2006) 205101.
[53] S. Grimme, Semiempirical GGA-type density-functional constructed with a long-range dispersion correction, J. Comput. Chem. 27 (2006) 1787–1799.
[54] N. Marom, A. Tkatchenko, M. Scheffler, L. Kronik, Describing both dispersion interactions and electronic structure using density functional theory: the case of metal–phthalocyanine dimers, J. Chem. Theory Comput. 6 (2010) 81–90.
[55] A. Tkatchenko, M. Scheffler, Accurate molecular Van der Waals interactions from ground-state electron density and free-atom reference data, Phys. Rev. Lett. 102 (2009) 073005.
[56] J.M. Blanco, C. González, P. Jelínek, J. Ortega, F. Flores, R. Pérez, First-principles simulations of STM images: from tunneling to the contact regime, Phys. Rev. B 70 (2004) 1–9.
[57] C. González, P. Snijders, J. Ortega, R. Pérez, F. Flores, S. Rogge, H. Weitering, Formation of atom wires on vicinal silicon, Phys. Rev. Lett. 93 (2004) 2–5.
[58] P. Snijders, S. Rogge, C. González, R. Pérez, J. Ortega, F. Flores, H. Weitering, Ga-induced atom wire formation and passivation of stepped Si(1 1 2), Phys. Rev. B 72 (2005) 1–12.
[59] P. Pou, R. Pérez, F. Flores, A. Yeyati, A. Martin-Rodero, J. Blanco, F. García-Vidal, J. Ortega, Local-density approach and quasiparticle-levels for generalized Hubbard Hamiltonians, Phys. Rev. B 62 (2000) 4309–4331.
[60] J. Fraxedas, S. García-Gil, S. Monturet, N. Lorente, I. Fernández-Torrente, K.J. Franke, J.I. Pascual, A. Völlmer, R.P. Blum, N. Koch, P. Ordejón, Modulation of surface charge transfer through competing long-range repulsive versus short-range attractive interactions, J. Phys. Chem. C 115 (2011) 18640–18648.